Characterization of vacancy-type defects in Mg- and N-implanted GaN by using a monoenergetic positron beam

Akira Uedono[1], Ryo Tanaka[2], Shinya Takashima[2], Katsunori Ueno[2], Masaharu Edo[2], Kohei Shima[3], Shigefusa F. Chichibu[3], Jun Uzuhashi[4], Tadakatsu Ohkubo[4], Shoji Ishibashi[5], Kacper Sierakowski[6], and Michal Bockowski[6]

[1]Institute of Pure and Applied Science, University of Tsukuba, Tsukuba, Ibaraki 305-8573, Japan
[2]Advanced Technology Lab., Fuji Electric Co., Ltd., Hino, Tokyo 191-8502, Japan
[3]Institute of Multidisciplinary Research for Advanced Materials, Tohoku University, Sendai 980-8577, Japan
[4]National Institute for Materials Science, Tsukuba 305-0047, Japan
[5]Research Center for Computational Design of Advanced Functional Materials, National Institute of Advanced Industrial Science and Technology, Tsukuba, Ibaraki 305-8568, Japan
[6]Institute of High Pressure Physics, Polish Academy of Sciences, Sokolowska 29/37, 01-142 Warsaw, Poland

1. Introduction

Gallium nitride (GaN) is one of the key materials for post-Si-based power electronics. At present, almost all commercial GaN-based devices are fabricated using lateral architecture. However, high-performance vertical GaN diodes and transistors have been studied extensively [1-4]. Here, optimization of the device processing is key for commercializing vertical devices. One of the critical building blocks for these devices is the selective area doping of impurities. Precisely controlled impurity concentrations and their profiles can be done using only ion implantation. The major drawback of ion implantation is the generation of point defects due to atomic collisions [5]. Such defects could relate to the low activation rate of implanted impurities, the degradation of electric properties, and the reliability of devices.

It is well known that activating Mg implanted into GaN is difficult [6,7]. One of the reasons for this was the presence of donor-like point defects such as nitrogen vacancies (V_N). Additional implantation of N into Mg-implanted GaN was reported to be effective in enhancing the activation rate of implanted Mg [8]. However, the reactions of point defects and the formation process of secondary defects, such as dislocations, precipitates, and stacking faults, are unknown. Positron annihilation spectroscopy is a useful technique for detecting vacancy-type defects in solids. This technique has been used to study native and process-induced defects in GaN [9–12]. In the present study, we used a monoenergetic positron beam to study the annealing behaviors of vacancy-type defects in Mg- and N-implanted GaN.

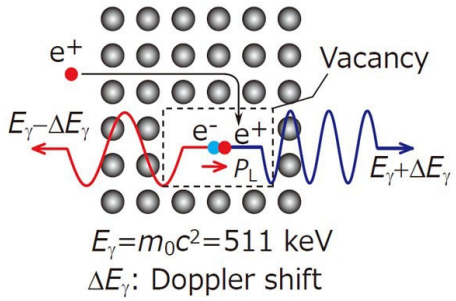

Fig. 1. Positron annihilates with an electron, and annihilation γ rays. When positrons are implanted into solids, they could be trapped by vacancy-type defects. One can detect vacancies from measurements of the energy distribution of γ rays.

2. Positron annihilation spectroscopy

When a positron is implanted into solids, it annihilates with an electron and emits γ quanta [13]. The momentum component of the annihilating electron-positron pair broadens the energy distribution of the γ rays. A positron could be trapped by a vacancy because of Coulomb repulsion from ion cores (Fig. 1). Because the momentum distribution of the electrons in the defects differs from that of electrons in the bulk, the defects can be detected by measuring Doppler broadening spectra of the annihilation radiation. The change in the spectra due to the positron trapping is shown in Fig. 2. The spectra are characterized by the *S* and *W* parameters defined as the fraction of annihilation events in the central and wing regions, respectively. The value of *S* (*W*) tends to increase with increasing (decreasing) the size of vacancy-type defects.

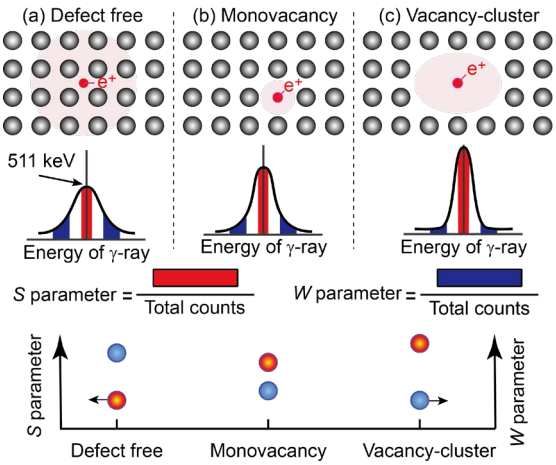

Fig. 2. Schematic drawing of Doppler broadening spectrum for (a) annihilation of positrons in delocalized state and trapped by (b) monovacancy and (c) vacancy cluster. The *S* and *W* parameters characterize the spectrum.

3. Experimental

The samples were undoped GaN grown on GaN substrates by metal-organic vapor phase deposition (MOVPE). Mg ions were implanted with 10 to 700 keV to obtain a 700-nm-deep box profile with a concentration ([Mg]) of 1×10^{18} cm^{-3}. After the implantation, N ions were implanted, and their depth profile was set to be similar to that of Mg, and its concentration in the box profile was 1×10^{18} cm^{-3}. N ion-implanted samples without Mg-implantation were also prepared. After the implantation, the samples were annealed at temperatures between 1000°C and 1450°C for 5 minutes under an N_2 pressure of 1 GPa [14].

The present samples were characterized by using a monoenergetic positron beam. Details on this technique are given elsewhere [13]. The Doppler broadening spectra were measured using Ge detectors as a function of the incident positron energy E. The relationship between the S parameter and E was analyzed using the computer code VEPFIT [15]. The Doppler broadening spectra were simulated by QMAS (Quantum MAterials Simulator) code [16] based on the projector augmented-wave (PAW) method [17] and a plane-wave basis set. Details on applying QMAS to calculations of positron states and annihilation parameters in group-III nitrides are given elsewhere [18].

4. Results and Discussion

Figure 3 shows the S values of the Mg-implanted GaN with N-implantation before and after annealing as a function of E. The mean implantation depth of positrons is shown on the upper horizontal axis. The S value corresponding to the annihilation of positrons from the delocalized state (S_f) was 0.442. The S value at $E\cong0.1$ keV is due to the annihilation of positrons at the surface. For the as-implanted sample, the S values at $E>1$ keV were higher than S_f, suggesting the trapping of positrons by vacancies introduced by the ion implantation. The S values for the damaged region (E=1–15 keV) were increased by annealing at 1000°C, and they started to decrease above 1100°C annealing. For the sample annealed above 1300°C, the S value was almost close to S_f, suggesting that the trapping of positrons by vacancy-type defects is negligible.

The solid curves shown in Fig. 3 are fits to the experimental data. Figure 4 shows the derived depth distributions of S. The depth profiles of Mg were measured by secondary ion mass spectrometry (SIMS), and the results are also shown in Fig. 2. No significant change in the Mg profiles was observed before and after annealing, and the depth profiles of vacancy-type defects and Mg agreed on each other. For the sample annealed at 1000°C, the increase in S occurred below 700 nm, and this region agreed with the box profile of Mg, suggesting that the agglomeration of vacancy-type defects mainly occurred in the high Mg concentration region.

Figure 5 shows the annealing behavior of the S value measured by the coincidence Doppler broadening technique at E=5 keV [13]. It shows that the decrease in the S value started above 1100°C annealing. The spectra were also

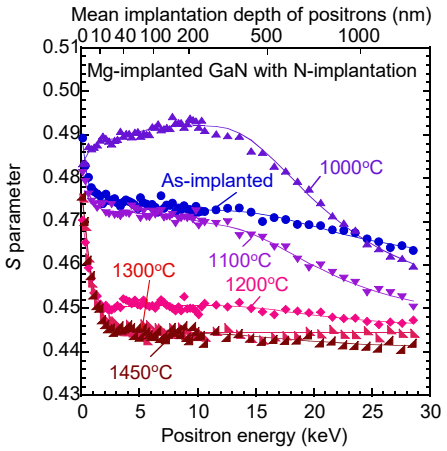

Fig. 3. S parameters as function of incident positron energy E for Mg-implanted GaN with N-implantation before and after annealing at 1000–1400°C. Solid curves are fits to experimental data.

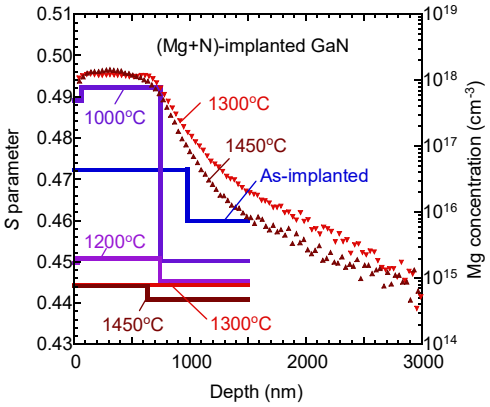

Fig. 4. Depth distributions of S obtained from analysis of S–E curves shown in Fig. 3 and depth distributions of Mg implanted into GaN.

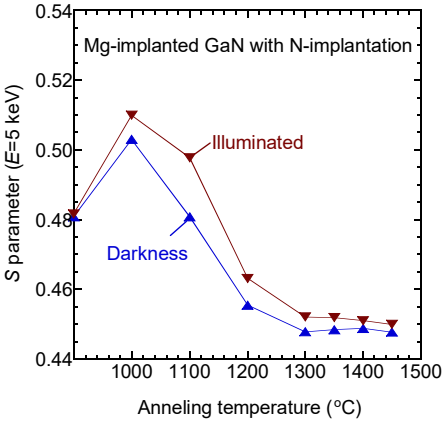

Fig. 5. S parameter measured at E = 5 keV as a function of annealing temperature for Mg-implanted GaN with N-implantation. Measurements were performed in darkness and under illumination.

measured under the illumination of a 325-nm He-Cd laser. The difference between the S values measured in darkness and under illumination can be attributed to the change in the charge state of vacancy-type defects by the illumination [9-

12]. Because positrons are repelled from positively charged defects, they are not detected by positron annihilation [13]. With the increase in annealing temperature, Mg could be partially activated, and this causes a change in the charge states of vacancy-type defects from neutral to positive. These defects are likely to act as electron-trapping centers and can be detected after capturing electrons excited by the illumination.

Figures 6 and 7 show *S*–*W* relationships for the Mg-implanted GaN with N-implantation and N-implanted GaN obtained from the coincidence Doppler broadening spectra (brown and pink symbols), respectively. During the measurements, the value of *E* was fixed at *E*=5 keV. The (*S*,*W*) value corresponding to the positron annihilation in a delocalized state is shown as "DF" (defect-free). The (*S*,*W*) value calculated from the simulated spectrum for the delocalized state is shown as "DF(cal.)." The simulated (*S*,*W*) values for typical vacancy-type defects are also shown in the figures (blue symbols).

For the N-implanted GaN before annealing (As-imp.), the value measured in darkness was close to the values for V_{Ga} and $V_{Ga}V_N$. Thus, the major defect species in the as-implanted sample can be identified as V_{Ga}-type defects. After annealing at 1000–1100°C, the value shifted to the right-hand side, suggesting the agglomeration of vacancy-type defects. After 1200°C annealing, however, the (*S*,*W*) value shifted towards the left-hand side, and the values for the samples annealed at 1300 and 1400°C were located on the line (brown) connecting the values for DF and the sample before annealing. From the observed annealing behavior of the (*S*,*W*) value, it can be concluded that the shrinkage of vacancy-type defects starts above 1200°C, and this can be attributed to recombinations between vacancy clusters and excess N atoms. The result suggests that N sequential implantation effectively suppresses the agglomeration of vacancies, but one needs to anneal the sample at least above 1200°C to obtain this effect.

For the Mg-implanted GaN with N-implantation, the clustering of vacancies was observed after 1000°C annealing, where the behavior of the (*S*,*W*) value was similar to that for N-implanted GaN. Above 1100°C, the (*S*,*W*) value approached the defect-free value along with the line connecting the values of DF(cal.) and $(V_{Ga}V_N)_3$, suggesting that the major defect species above 1100°C was vacancy clusters, and no change in the defect species was observed by annealing.

As shown in Figs. 6 and 7, for both ion-implanted GaN, the (*S*,*W*) values tended to show a righthand shift under the illumination. The increase in the number of V_N coupled with V_{Ga} causes the righthand shift in the *S*–*W* plot. Thus, the vacancy clusters acting as the electron trapping centers are considered to have more V_N than neutral or negatively charged clusters detected in darkness.

Figure 8 shows images of the (a) Mg-implanted GaN with N-implantation and (c) N-implanted GaN after annealing at 1400°C obtained by low-angle annular dark-field scanning transmission electron microscopy (LAADF-STEM). Their

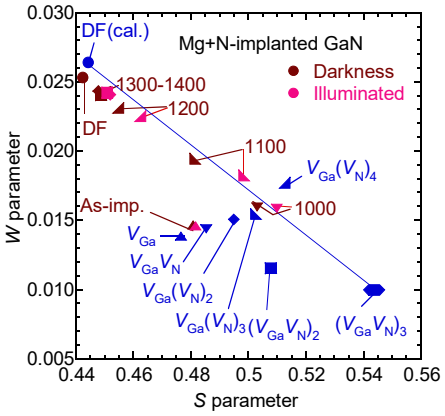

Fig. 6. *S*–*W* relationships measured in darkness (brown symbols) and under illumination (pink symbols) for Mg-implanted GaN with N-implantation. (*S*,*W*) for un-implanted GaN is shown as "DF" (defect-free). The value obtained by simulations for defect-free GaN [DF(cal.)], V_{Ga}, $V_{Ga}(V_N)_n$ (n=1–4), and $(V_{Ga}V_N)_m$ (m=2,3) are shown as blue symbols.

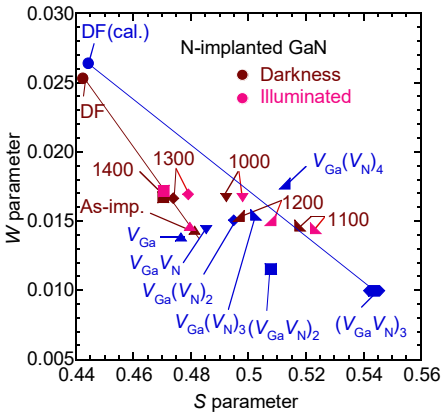

Fig. 7. *S*–*W* relationships measured in darkness and under illumination for N-implanted GaN. Simulated values for vacancy-type defects are shown as blue symbols.

magnified images are shown in (b) and (d), respectively. Bright dots were observed in the N-implanted sample. Their origin has been attributed to nano-scale intrinsic defects [19,20]. For the Mg-implanted sample with N-implantation, both bright dots and circles were observed. The nature of the later defects was identified as collapsed vacancy disks forming intrinsic dislocation loops [19,20]. Since the formation of such dislocation loops requires the removal of both Ga and N atoms from the inside of the loops, the V_{Ga}-rich condition for the N-implanted GaN is considered to be the origin of the suppression of the formation of such secondary defects.

5. Conclusions

Annealing behaviors of vacancy-type defects in ion-implanted GaN were studied by positron annihilation. For as-implanted samples, the major defect species was identified as V_{Ga}-type defects. For N-implanted GaN, the size of the vacancies increased as the annealing temperature

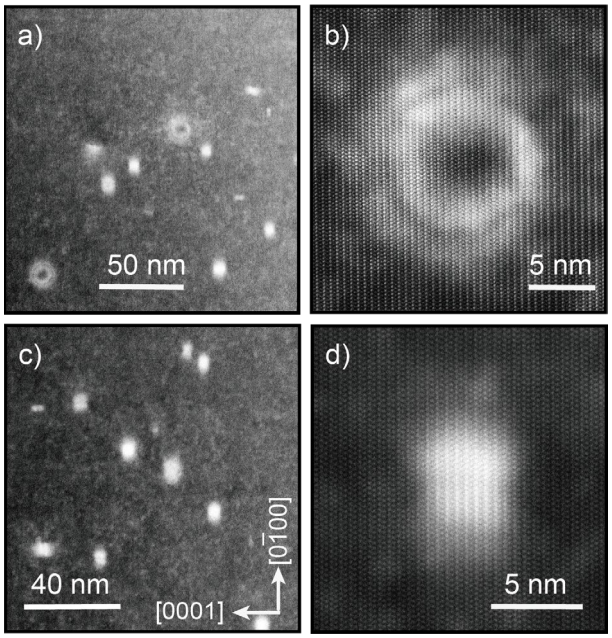

Fig. 8. LAADF-STEM images of (a) Mg-implanted GaN with N-implantation, (c) N-implanted GaN. Their magnified images are shown in (b) and (d), respectively. All samples were annealed at 1400°C.

increased up to 1100°C and then shrunk above 1200°C. This behavior was attributed to recombinations between V_N-type defects and excess N. For Mg-implanted GaN with N-implantation, the major defect species after annealing above 1000°C was vacancy clusters such as $(V_{Ga}V_N)_3$. Positively charged vacancy clusters were formed after annealing above 1000°C, and they have more V_N than neutral or negatively charged clusters. After annealing at 1400°C, the major secondary defects were nano-scale intrinsic defects and collapsed vacancy disks forming intrinsic dislocation loops, and the formation of the latter defects was suppressed in N-implanted GaN.

Acknowledgments

This work was supported in part by the NEDO Program for Cross-Ministerial Strategic Innovation Promotion, the MEXT Program for Research and Development of Next-Generation Semiconductor to Realize Energy-Saving Society (grant no. JPJ005357), the MEXT Program for Creation of Innovative Core Technology for Power Electronics (grant no. JPJ009777), and JSPS KAKENHI (grant no. 21H01826). This research was also partially supported by the Polish National Centre for Research and Development through project TECHMATSTRATEG-III/0003/2019-00 and Polish National Science Centre through project 2018/29/B/ST5/00338.

References

[1] J. Hu, Y. Zhang, M. Sun, D. Piedra, N. Chowdhury, and T. Palacios, Mat. Sci. Semicond. Process. 78, 75 (2018).
[2] T. Oka, Jpn. J. Appl. Phys. 58. SB0805 (2019).
[3] Y. H. Zhang, A. Dadgar, and T. Palacios. J. Phys. D: Appl. Phys. 51, 273001 (2018).
[4] T. Narita, H. Yoshida, K. Tomita, K. Kataoka, H. Sakurai, M. Horita, M. Bockowski, N. Ikarashi, J. Suda, and T. Kachi, and Y. Tokuda, J. Appl. Phys. 128, 090901 (2020).
[5] S. O. Kucheyev, J. S. Williams, S. J Pearton, Mat. Sci. Eng. Rep. 33, 51 (2001).
[6] T. Kachi, T. Narita, H. Sakurai, M. Matys, K. Kataoka, K. Hirukawa, K. Sumida, M. Horita, N. Ikarashi, K. Sierakowski, M. Bockowski, J. Suda, J. Appl. Phys. 132, 130901 (2022).
[7] A. Ferreyra, B. J. Li, S. Z. Wang, J. Han, J. Phys. D 56, 373001 (2023).
[8] R. Tanaka, S. Takashima, K. Ueno, H. Matsuyama, M. Edo, Jpn. J. Appl. Phys. 59, SGGD02 (2020).
[9] A. Uedono, H. Sakurai, T. Narita, K. Sierakowski, M. Bockowski, J. Suda, S. Ishibashi, S. F. Chichibu, and T. Kachi, Sci. Rep. 10, 17349 (2020).
[10] A. Uedono, R. Tanaka, S. Takashima, K. Ueno, M. Edo, K. Shima, K. Kojima, S. F. Chichibu, and S. Ishibashi, Sci. Rep. 11, 20660 (2021)
[11] A. Uedono, H. Sakurai, J. Uzuhashi, T. Narita, K. Sierakowski, S. Ishibashi, S. F. Chichibu, M. Bockowski, J. Suda, T. Ohkubo, N. Ikarashi, K. Hono, and T. Kachi, Phys. Stat. Sol. B 259, 2200183 (2022).
[12] A. Uedono, R. Tanaka, S. Takashima, K. Ueno, M. Edo, K. Shima, S. F. Chichibu, J. Uzuhashi, T. Ohkubo, S. Ishibashi, K. Sierakowski, and M. Bockowski, Phys. Stat. Sol. B 261, 2400060 (2024).
[13] R. Krause-Rehberg, H. S. Leipner, Positron Annihilation in Semiconductors, Solid-State Sciences vol. 127, Springer-Verlag, Berlin, 1999.
[14] K. Sierakowski, R. Jakiela, B. Lucznik, P. Kwiatkowski, M. Iwinska, M. Turek, H. Sakurai, T. Kachi, M. Bockowski, Electronics, 9, 1380 (2020).
[15] A. Van Veen, H. Schut, M. Clement, J. M. M. de Nijs, A. Kruseman, M. R. IJpma, Appl. Surf. Sci., 85, 216 (1995).
[16] S. Ishibashi, T. Tamura, S. Tanaka, M. Kohyama, K. Terakura, Phys. Rev. B 76, 153310 (2007).
[17] P. E. Blochl, Phys. Rev. B 50, 17953 (1994).
[18] S. Ishibashi, A. Uedono, H. Kino, T. Miyake, and K. Terakura, J. Phys. Cond. Matt. 31, 475401 (2019).
[19] K. Iwata, H. Sakurai, S. Arai, T. Nakashima, T. Narita, K. Kataoka, M. Bockowski, M. Nagao, J. Suda, T. Kachi, N. Ikarashi, J. Appl. Phys., 127, 105106 (2020).
[20] E. Kano, K. Kataoka, J. Uzuhashi, K. Chokawa, H. Sakurai, A. Uedono, T. Narita, K. Sierakowski, M. Bockowski, R. Otsuki, K. Kobayashi, Y. Itoh, M. Nagao, T. Ohkubo, K. Hono, J. Suda, T. Kachi, N. Ikarashi, J. Appl. Phys., 132, 065703 (2022).